THE JOURNAL OF PHYSICAL CHEMISTRY C

Article

Frustrated Triangular Magnetic Structures of MnZnN: Applications in Thermal Expansion

Sihao Deng, Ying Sun, Lei Wang, Zaixing Shi, Hui Wu, Qing-Zhen Huang, Jun Yan, Kewen Shi, Pengwei Hu, Ali Zaoui, and Cong Wang

J. Phys. Chem. C, **Just Accepted Manuscript** • DOI: 10.1021/acs.jpcc.5b07225 • Publication Date (Web): 07 Oct 2015

Frustrated Triangular Magnetic Structures of Mn_3ZnN: Applications in Thermal Expansion

Sihao Deng,[1] Ying Sun,[1,*] Lei Wang,[1] Zaixing Shi,[1] Hui Wu,[2] Qingzhen Huang,[2] Jun Yan,[1] Kewen Shi,[1] Pengwei Hu,[1] Ali Zaoui,[3] Cong Wang,[1,*]

[1] *Center for Condensed Matter and Materials Physics, Department of Physics, Beihang University, Beijing 100191, People's Republic of China*

[2] *NIST Center for Neutron Research, National Institute of Standards and Technology, Gaithersburg, Maryland 20899-6102, United States*

[3] *LGCgE-Lille Nord de France, Polytech'Lille, Université de Lille1 Sciences et Technologies, 59655 Villeneuve d'Ascq, France*

* Corresponding author. E-mail: sunying@buaa.edu.cn.

E-mail: congwang@buaa.edu.cn.

ABSTRACT:

One of the specific subjects in frustrated magnetic systems is the phenomenon coupled with noncollinear magnetism, such as zero or negative thermal expansion (ZTE or NTE) in antiperovskite compounds. The first-principles calculations and neutron powder diffraction (NPD) are used to reveal the control of the noncollinear Γ^{5g} antiferromagnetic (AFM) structure and corresponding thermal expansion properties in $Mn_3Zn_{0.875}X_{0.125}N$ (X = Mn, Ge, and Sn). Based on the optimal exchange-correlation functional, our results demonstrate that X (X = Mn, Ge, and Sn) doping at Zn site could stabilize the noncollinear Γ^{5g} AFM structure and produce magnetovolume effect (MVE). The predictions of Γ^{5g} AFM ground state and MVE is further verified by the NPD results of $Mn_3Zn_{0.83}Mn_{0.15}N_{0.99}$. Intriguingly, this special magnetic structure with strong spin-lattice coupling can be tunable to achieve ZTE behavior. On the basis of these results we suggest that frustrated magnetic systems with noncollinear Γ^{5g} AFM structure of Mn atoms in Mn_3ZnN series of compounds are favorable candidates for a new class of ZTE material.

KEYWORDS: noncollinear magnetism, thermal expansion, spin-lattice coupling, antiperovskite

1. INTRODUCTION

Recent years, frustrated magnetic systems, in which competing interactions between spins preclude simple magnetic orders, have become a stimulating research topic because of the presence of extraordinary magnetic properties such as highly degenerate ground states, novel phase transitions, and noncollinear ordering.[1-7] One of the specific subjects in this field is the phenomenon coupled to noncollinear magnetism. For example, the multiferroic behaviors, caused by an incommensurate cycloidal order combined with spin-orbit coupling, was found in manganite perovskites $RMnO_3$ (such as R = Tb and Dy).[8, 9] Also, colossal magnetoresistance and quantum anomalous Hall effects were observed due to the effect of unusual noncollinear and even noncoplanar spin textures.[10-12] Owing to such diversity of phenomena associated with noncollinear ordering, the exploration in models, materials, and artificial structures related to noncollinear ordering has developed into a very spirited field of investigation.[10, 13-15]

The triangular magnetic lattice is the most obvious example of geometrically frustrated magnetic system.[16] Notably, Mn-based antiperovskite compounds with triangular magnetic lattice show a variety of magnetic structures accompanied with fascinating physical properties. A large magnetic entropy change was observed near magnetic transition from paramagnetic (PM) to unusual magnetic state, such as P1 symmetry noncollinear ferrimagnetism (FIM) in $Mn_3Cu_{0.89}N_{0.96}$ and a canted ferromagnetic state in Mn_3GaC.[17-19] Giant magnetostriction was reported in the tetragonally distorted ferromagnetic phase of antiperovskite Mn_3SbN and Mn_3CuN.[20, 21] Besides, unusual magnetic hysteresis in $Mn_3Sb_{1-x}Sn_xN$ and giant magnetoresistance in Mn_3GaC were found.[22, 23] More importantly, the antiperovsktie compounds with noncollinear Γ^{5g} antiferromagnetic (AFM) structure where the Mn local magnetic moments on the (111) plane form clockwise or counterclockwise configuration show attractive behaviors, including giant barocaloric, flexomagnetic, piezomagnetic, Invar-like, and negative thermal expansion (NTE) etc.[24-29]

Among these manganese antiperovskites, Mn_3ZnN with Γ^{5g} AFM phase, which has the strong spin-lattice coupling, is one of the most promising material as a single compound displaying zero thermal expansion (ZTE) from the perspective of functionality and cost.[27, 30] Fruchart et al. reported that Mn_3ZnN was characterized by two distinct magnetic transitions: at 183 K, a high-temperature (high-T) PM state changes to an intermediate-T Γ^{5g} AFM state with a sudden lattice expansion upon cooling; with further cooling, another magnetic transition from Γ^{5g} AFM to low-T collinear AFM phases occurs at 140 K, accompanied with a sharp lattice contraction.[19, 31] Moreover, from the current neutron powder diffraction (NPD) result of $Mn_3Zn_{0.99}N$ reported by our group, the coexistence of Γ^{5g} AFM and low-T collinear AFM phases was observed in the intermediate-T region.[27] Recently, intermediate-T Γ^{5g} AFM phase that controls ZTE and has a larger volume (compared with PM phase) was found to be tunable by chemical substitution at Zn site, such as Ge or Sn.[27, 32, 33] On the other hand, reliable methods of the unconstrained noncollinear first-principles study was well established[34-36] and widely adopted for explaining and predicting physical properties of materials.[25, 34, 37] In this study, the first-principles study based on various exchange-correlation (EC) functionals has been developed in order to get the reasonable ground state of Mn_3ZnN. Based on the preferred EC functional PW91, both Γ^{5g} AFM ground state and magnetovolume effect (MVE) are confirmed in X doped $Mn_3Zn_{0.875}X_{0.125}N$ (X = Ge or Sn), which qualitatively agrees to the experimental results. The prediction that Mn doping at Zn site could induced the Γ^{5g} AFM ground state is verified from our NPD results of $Mn_3Zn_{0.83}Mn_{0.15}N_{0.99}$. Additionally, the observed ZTE behavior originated from spin-lattice coupling in Mn_3ZnN series of compounds with Γ^{5g} AFM phase provides a new feasible way to obtain ZTE materials.

2. COMPUTATIONAL AND EXPERIMENTAL METHODS

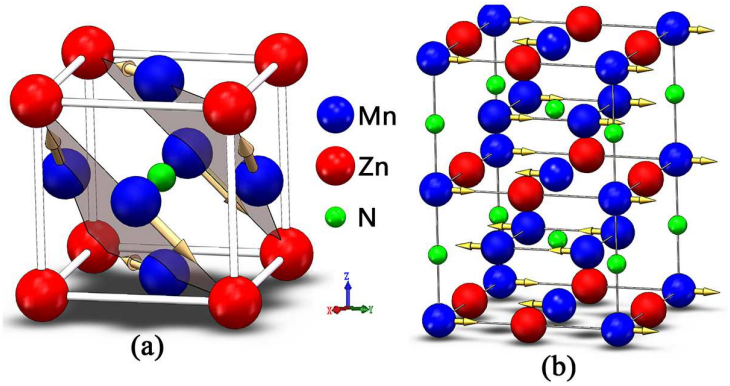

Figure 1. Crystal and magnetic phases of Mn_3ZnN for (a) antiperovskite crystal structure and noncollinear Γ^{5g} AFM and (b) collinear AFM structures.

Computational methods

Density functional theory (DFT) was performed here using the projector augmented-wave (PAW) method initially proposed by Blöchl.[38] For fully unconstrained noncollinear magnetic structures we used the execution of Kresse and Joubert[39] in Vienna *Ab-initio* Simulation Package (VASP) code within local density approximation (LDA)[37] and generalized gradient approximation (GGA)[25]. Among the available GGA functionals, we selected two commonly used and popular standard functionals PW91[40] and PBE[41], respectively. Besides, as specially developed functionals for calculations on solids and solid surfaces, AM05[42] and PBEsol[43] were also employed. The cutoff energy of 500 eV and Gamma-centered k points with a 3×3×3 grid were used. The noncollinear Γ^{5g} magnetic structure with the spins on the (111)-plane was applied. The nonmagnetic supercell with total magnetic moment being zero was adopted to mimic a high-temperature paramagnetic (PM) phase.[26] Based on the unit cell of Mn_3ZnN shown in Figure 1(a), a supercell containing 2×2×2 primitive unit cells was adopted. Furthermore, in order to get the composition of $Mn_3Zn_{0.875}X_{0.125}N$ (X = Mn, Ge, and Sn), the chemical formula $Mn_{40}Zn_7XN_8$ supercell was used in our calculations by the substitution of X for Zn

atom at the site (0.5, 0.5, 0.5).

The radial distribution function (RDF), g(r), is very important for studying the structure of $Mn_{40}Zn_7XN_8$. The RDF can be expressed as:

$$g(r)=\frac{N_n(r)V_n}{4\pi r^2 drN} \quad (1)$$

where $N_n(r)$ and V_n are the mean numbers and mean volume of atoms between r to $r+dr$ around an atom, N is the numbers of atoms.[44] For $Mn_{40}Zn_7XN_8$, after optimizing the structure using VASP code, the RDF (Zn/X-Mn around X) is calculated by the VMD software.[45]

Experimental methods

Polycrystalline sample of the nominal composition $Mn_3Zn_{0.80}N$ was prepared by solid-state reaction in vacuum (10^{-5} Pa) using Mn_2N and Zn (3N) as the starting materials.[27] The real composition determined by Rietveld analysis of NPD data at room temperature is $Mn_3Zn_{0.83}Mn_{0.15}N_{0.99}$. NPD data at 10 K to 250 K were collected using the BT-1 high-resolution neutron powder diffractometer at NIST Center for Neutron Research (NCNR). A Cu (311) monochromator was used to produce monochromatic neutron beam with wavelength of 1.5403 Å. The intensities were measured with a step of 0.05° in the 2θ range of 5°-162° to determine the crystal and magnetic structures and reveal thermal expansion properties. The crystal and magnetic structures were refined by Rietveld method with the General Structure Analysis System (GSAS) program.[46] The neutron scattering lengths used in the refinement were -0.375, 0.568, and 0.936 ($\times 10^{-12}$ cm) for Mn, Zn, and N, respectively. The crystal and magnetic structures of Mn_3ZnN are shown in Figure 1.[27]

3. RESULTS AND DISCUSSION

As shown in Figure 1(a), Mn_3ZnN possesses an antiperovskite crystal structure.[19, 27] The noncollinear Γ^{5g} AFM magnetic structure clarified by Fruchart[19] [see Figure 1(a)] was adopted for the simulation of Mn_3ZnN.[47] Table 1 lists the structural and

magnetic parameters of antiperovskite Mn_3ZnN obtained using different EC functionals with Γ^{5g} AFM magnetic structure. The calculated equilibrium lattice constants a_0 correspond to 3.702, 3.781 and 3.790 **Å** for the EC functionals LDA, AM05 and PBEsol, respectively, which are underestimated compared with the experimental value of 3.912 **Å** at 151 K in the literature.[27] Moreover, our calculated a_0 value is 3.860 **Å** for the case of PW91 and 3.871 **Å** for PBE functional, which is in good agreement with previously reported results, i.e., 3.912 Å. Similarly, the reasonable magnetic moments m of the Mn atoms, 2.60 μ_B/atom for PBE and 2.51 μ_B/atom for PW91, are close to the experimental value of 2.61 μ_B/atom at 151 K.[27] In particular, the values of a_0 and m using PBE are close to the previously calculated results 3.870 **Å** and 2.63 μ_B/atom.[47] These characteristics with diverse EC functionals indicate that PBE and PW91 are better than others for the current study of Mn_3ZnN.

Table 1. Results of the calculated equilibrium lattice constants a_0 and magnetic moment m with different EC functionals compared with experimental data.

	LDA	AM05	PBEsol	PBE	PW91	Experiment
a_0 (Å)	3.702	3.781	3.790	3.871, 3.870[44]	3.860	3.912[27]
m (μ_B)	2.21	2.10	2.16	2.60, 2.63[44]	2.51	2.61[27]

As referred above, Mn_3ZnN shows phase separation behavior [collinear AFM shown in Figure 1(b) and Γ^{5g} AFM phases] from 140 K to 177 K.[48] Herein, the collinear AFM phase is marked as M_{PTE} in Figure 1(b) as the positive thermal expansion (PTE) behavior was observed within this magnetic structure.[27] Next, we will focus on the discussion of both Γ^{5g} and M_{PTE} AFM phases using the PBE and PW91 EC functionals. It was found that the cases of PW91 and PBE EC functional show different ground states. The total energy of the Mn_3ZnN as a function of the lattice constant for Γ^{5g} and M_{PTE} AFM phases are shown in Figure 2. As seen from

Figure 2(a), the total energy of the Γ^{5g} magnetic structure is 0.008 eV/f.u. (f.u. is the abbreviation of formula unit) lower than that of the M_{PTE} state at their optimal lattices using PBE, which is qualitatively in agreement with the previously calculated results.[47] This indicates that magnetic ground state is Γ^{5g} AFM structure in the case of PBE EC functional. However, instead of Γ^{5g} AFM phase, the M_{PTE} ground state should be observed because this phase was confirmed below 140 K from NPD result.[27, 48] Importantly, as shown in Figure 2(b), the M_{PTE} ground state is obtained in the case of PW91, indicating the PW91 EC functional should be selected for the simulation of Mn_3ZnN.

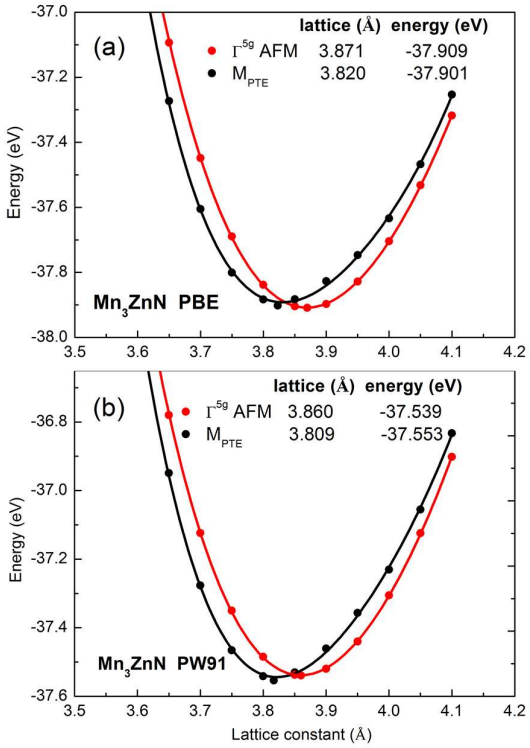

Figure 2. Total energy of the Mn_3ZnN as a function of the lattice constant for Γ^{5g} AFM and M_{PTE} phases using (a) PBE and (b) PW91 EC functionals.

Based on the calculated results by PW91 EC functional, the total energy of the M_{PTE} 0.014 eV/f.u. is lower than that of Γ^{5g} AFM state at their optimal lattices. Generally, phase separation behavior can be resulted from the thermodynamic competition between phases with nearly identical free energies.[48, 49] For Mn_3ZnN,

the total energy of Γ^{5g} AFM phase and that of M_{PTE} phase is close, and the energy difference 0.014 eV/f.u. is far less than those (similar energy difference) in other antiperovskite compounds (0.463 eV/f.u. for $Mn_{3.25}Ni_{0.75}N$[26] and 0.22 eV/f.u. for Mn_3GaN[25]) without phase separation phenomenon. Therefore, the phase separation observed between 140 K and 177 K might be attributed to the competition between Γ^{5g} AFM and M_{PTE} phases due to the nearly identical energy of both phases. On the other hand, the equilibrium lattice constant of the M_{PTE} state is 3.809 Å in the case of PW91, which implies a lattice contraction of 0.051 Å ($\Delta a/a = 0.013$) from the Γ^{5g} to M_{PTE} AFM state. This qualitatively agrees with the observed $\Gamma^{5g} \rightarrow M_{PTE}$ first-order phase transition in Mn_3ZnN with a $\Delta a/a$ of $\sim$0.006.[27] The calculated value of $\Delta a/a$ is slightly greater than the observed values. However, it does not affect the qualitative analysis of phase transition because such disagreement always exists in the current density functional theory calculation of antiperovskite compounds.[25, 26]

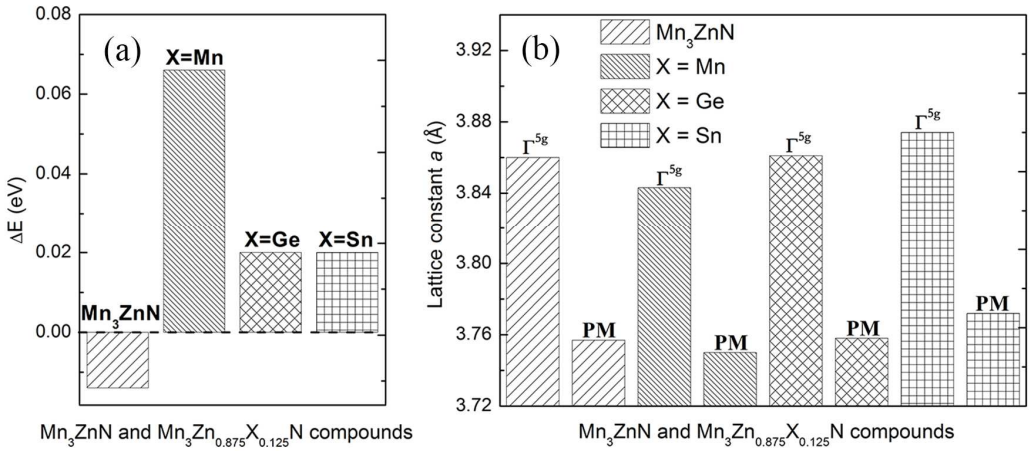

Figure 3. (a) The energy difference ΔE between $E_{M_{PTE}}$ and $E_{\Gamma}{}^{5g}$ ($E_{M_{PTE}}$-$E_{\Gamma}{}^{5g}$) and (b) the equilibrium lattice constant *a* of Γ^{5g} AFM and PM phases for Mn_3ZnN and $Mn_3Zn_{0.875}X_{0.125}N$ (X= Mn, Ge, and Sn) compounds using PW91 EC functional.

To further study the control of these two magnetic structures, the X doping at Zn site is adopted as $Mn_3Zn_{0.875}X_{0.125}N$ (X = Mn, Ge, and Sn). Based on the results of total energy at equilibrium lattice displayed in Figure S1, Figure 3(a) shows the

energy difference ΔE between $E_{M_{PTE}}$ and $E_{\Gamma}{}^{5g}$ for Mn_3ZnN and $Mn_3Zn_{0.875}X_{0.125}N$ (X= Mn, Ge, and Sn) using PW91 EC functional. Negative ΔE indicates that the M_{PTE} AFM phase is favorable; otherwise Γ^{5g} AFM structure should be stable. It can be seen that the ΔE values change from negative to positive with X doping at Zn sites, corresponding to -0.014, 0.066, 0.02, and 0.02 eV for Mn_3ZnN, $Mn_3Zn_{0.875}Mn_{0.125}N$, $Mn_3Zn_{0.875}Ge_{0.125}N$, and $Mn_3Zn_{0.875}Sn_{0.125}N$, respectively. This suggests that X doping could stabilize the special Γ^{5g} AFM phase as the ground state in $Mn_3Zn_{0.875}X_{0.125}N$. Moreover, as shown in Figure 3(b), the equilibrium lattice constants of Γ^{5g} AFM phase are 3.861 Å and 3.874 Å for Ge doped and Sn doped compounds, respectively, which are comparable to the experimental values of 3.909 Å for $Mn_3Zn_{0.9}Ge_{0.1}N$ at 202 K[32] and 3.930 Å for $Mn_3Zn_{0.8}Sn_{0.2}N$ at 265 K[33]. The calculated lattice constants of the PM phase become 3.758 Å for $Mn_3Zn_{0.875}Ge_{0.125}N$ and 3.772 Å for $Mn_3Zn_{0.875}Sn_{0.125}N$, signifying that the lattice contraction ($\Delta a/a$) 0.027 for Ge doping and 0.026 for Sn doping could be observed with magnetic transition from Γ^{5g} AFM to PM phase. These characteristics qualitatively agrees to the experimental results, e.g., antiperovskite compounds $Mn_3Zn_{1-x}X_xN$ with X (X = Ge and Sn) doping have been found to contain Γ^{5g} AFM ground state and exhibit NTE (ZTE) behavior that caused by MVE effect.[27, 32, 33] This suggests that we could make a prediction on the antiperovskite compounds with Γ^{5g} AFM ground state using PW91 EC functional. On the other hand, for Mn doped $Mn_3Zn_{0.875}Mn_{0.125}N$, the Γ^{5g} AFM ground state and MVE effect are also predicted, which will be discussed in the following experimental section.

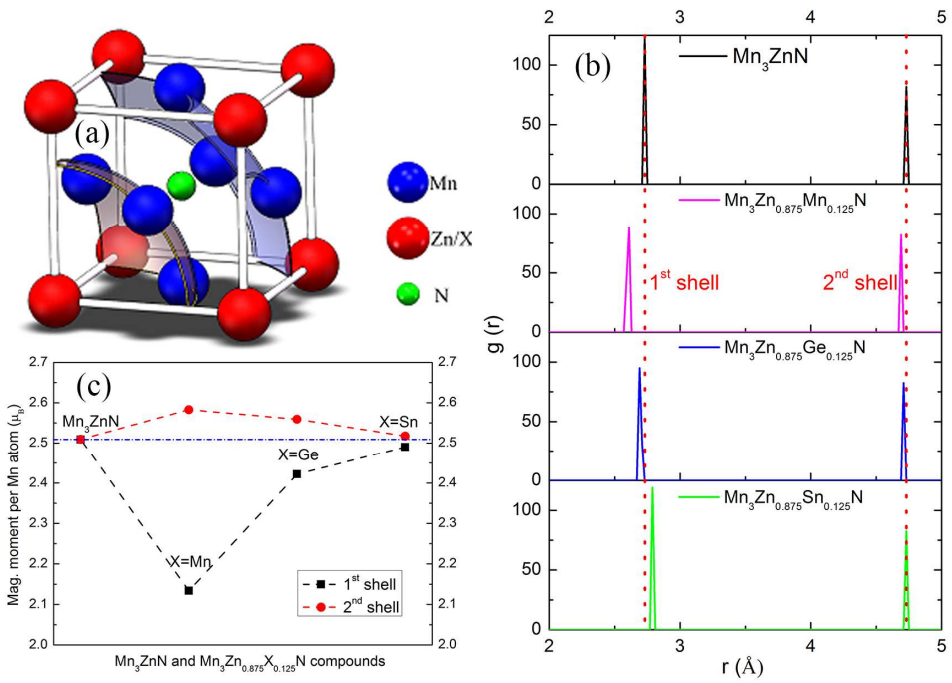

Figure 4. (a) Crystal structure showing the first (1^{st}) and second (2^{nd}) nearest shells (Zn/X-Mn) around X atom for Mn_3ZnN and $Mn_3Zn_{0.875}X_{0.125}N$ (X= Mn, Ge, and Sn). (b) Corresponding radial distribution function and (c) magnetic moment per Mn atom for 1^{st} and 2^{nd} shells.

The M_{PTE}-Γ^{5g} AFM (collinear-noncollinear) phase transition induced by X doping at Zn positions inspires us to explore the influence of doping on the structural changes in $Mn_3Zn_{0.875}X_{0.125}N$ (X = Mn, Ge, and Sn) because the magnetic phase transitions led by degenerating spin states around the ground state might be found due to the local lattice distortion.[16, 50] The RDF of the first (1^{st}) and the second (2^{nd}) nearest shells (Zn-Mn, Mn-Mn, Ge-Mn, and Sn-Mn) around X atom for Mn_3ZnN and $Mn_3Zn_{0.875}X_{0.125}N$ (X= Mn, Ge, and Sn) are shown in Figure 4(b). For the 1^{st} shell, the peaks are weakened and the shift of peak position occurs with X doping in Mn_3ZnN. These characteristics indicate that the geometrical distortion could be produced by X doping at Zn sites. However, only the tiny change is found with X doping for the 2^{nd} shell, implying that the geometrical distortion induced by doping could mainly locate near the doped site. On the other hand, the magnetic moment per Mn atom for the 1^{st} and 2^{nd} shells is shown in Figrue 4(c). It can be seen that the X doping has more

influence on Mn magnetic moment in the 1st shell compared with those in the 2nd shell. For the 1st shell, the values of Mn magnetic moment m_{Mn} are 2.13, 2.42 and 2.49 μ_B/Mn for X = Mn, Ge, and Sn, respectively, smaller than 2.51 μ_B/Mn in Mn_3ZnN. However, slightly larger values of 2.58, 2.56, and 2.52 μ_B/Mn are observed for $Mn_3Zn_{0.875}Mn_{0.125}N$, $Mn_3Zn_{0.875}Ge_{0.125}N$, and $Mn_3Zn_{0.875}Sn_{0.125}N$, respectively, in the 2nd shell. Notably, in antiperovskite compounds, the spin-lattice coupling of the Γ^{5g} AFM phase was confirmed by NPD results.[26, 27] Moreover, a decrease in the Mn magnetic moment (unpaired Mn 3*d* electrons) was found with Ge doping due to Ge 4*p* - Mn 3*d* orbital hybridization.[51] For the compounds with Mn doping, the contraction (relative expansion) of the 1st (2nd) shell caused by geometrical distortion may be coupled to Mn magnetic moment, resulting in the decrease (increase) of m_{Mn}. For $Mn_3Zn_{0.875}Ge_{0.125}N$ and $Mn_3Zn_{0.875}Sn_{0.125}N$, the tiny variation of m_{Mn} in the 2nd shell is observed with insignificant geometrical distortion, while the deceasing m_{Mn} in the 1st shell might be produced by the contribution from *p-d* (Ge 4*p* - Mn 3*d*, Sn 5*p* - Mn 3*d*) orbital hybridization and the spin-lattice coupling. However, details of these complicated contributions still need further investigations. Furthermore, combined with the discussions of the magnetic moment changes induced by X doping, some detailed analyses for the geometrical distortion of $Mn_3Zn_{0.875}X_{0.125}N$ are shown in the Support Information.

The M_{PTE}-Γ^{5g} AFM phase transition with X doping will be studied based on local lattice distortion. Firstly, we will focus on the nature of M_{PTE} in Mn_3ZnN. Generally, the simply collinear antiferromagnetic ordering is impossible in a two-dimensional triangular lattice.[52] We suggest that the M_{PTE}, which AFM lays are perpendicular to c axis, might be formed by the effect of the anisotropy energy in Mn_3ZnN. Similarly, as a typical material of triangular lattice antiferromagnet, $CuFeO_2$ forms an Ising-like 4-sublattice (↑↑↓↓) collinear AFM ordering due to the effect of the anisotropy energy when the easy-axis anisotropy is sufficiently large.[1, 7, 10, 16, 52, 53] Noticeably, these collinear AFM orderings are contrary to the typical noncollinear ordered structure of

triangular lattice antiferromagnet where the three spins align at 120° from each other in the basal plane, such as the Γ^{5g} AFM phase in Mn_3ZnN.[1, 54] Moreover, the spin-wave softening may be found as the collinear-noncollinear magnetic phase transition occurs in triangular lattice antiferromagnet. For the typical material $CuFeO_2$, The spin-wave gap is observed to decrease by substituting Al^{3+} ions for Fe^{3+}. When the Al concentration is greater than 1.6%, the collinear AFM phase becomes unstable and a noncollinear phase appears.[52, 55, 56]. Additionally, it is clear that the local lattice distortion caused by the difference of ionic radii between the doped element (e.g. Al^{3+}) and Fe^{3+} significantly affects the spin states in $CuFe_{1-x}Ga_xO_2$.[50] Therefore, it is proposed that, for geometrically frustrated $Mn_3Zn_{0.875}X_{0.125}N$, a similar spin-wave softening accompanied by local lattice distortion might be observed due to X doping, which could lead to the collinear-noncollinear magnetic phase transition.

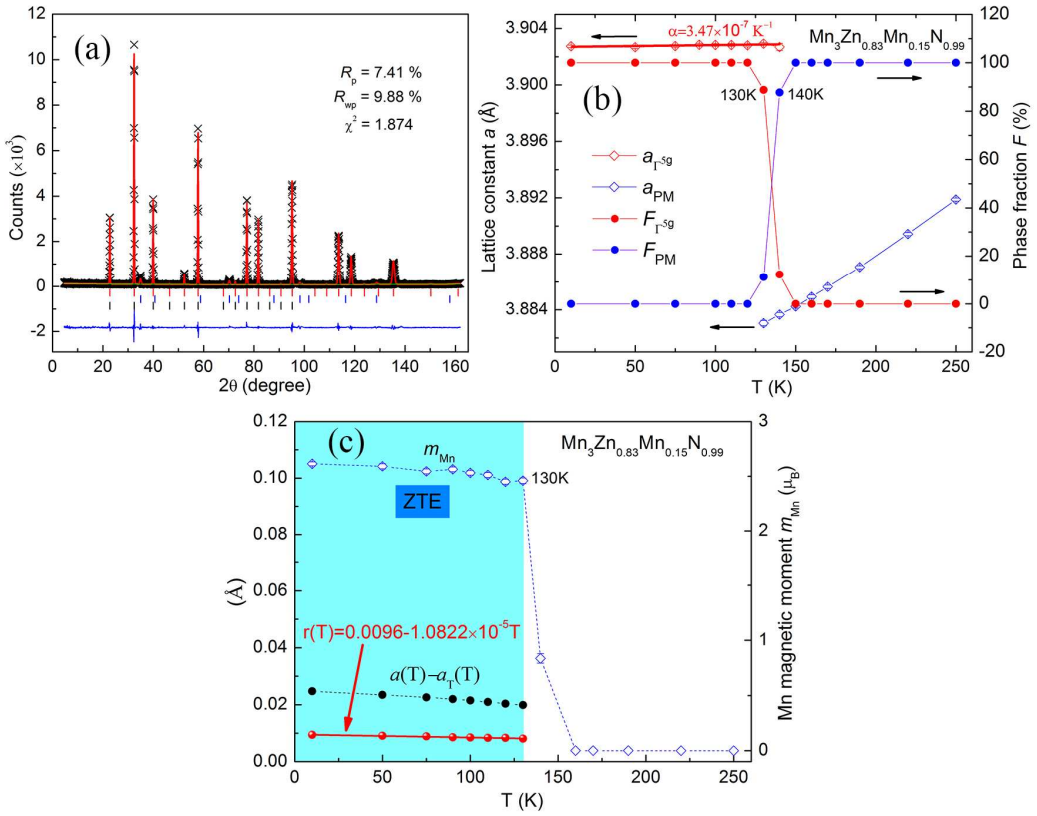

Figure 5. (a) Neutron powder diffraction patterns of $Mn_3Zn_{0.83}Mn_{0.15}N_{0.99}$ at 10 K. The crosses

show the experimental intensities (I_{obs}), the upper solid line shows the calculated intensities (I_{calc}), and the lower solid line is the difference between the observed and calculated intensities (I_{obs}-I_{calc}). The vertical lines indicate the angular positions of the nuclear (top row), MnO (second row), and the magnetic (third row) Bragg reflections. (b) Relationship between the lattice variation and phase fractions for the sample $Mn_3Zn_{0.83}Mn_{0.15}N_{0.99}$. Solid symbols represent phase fractions and open symbols depict lattice constants. Curves are guides to the eye. (c) Temperature dependence of the lattice variation a(T)-a_T(T), ordered magnetic moments (m_{Mn}) of the Γ^{5g} AFM structure, and r(T) for $Mn_3Zn_{0.83}Mn_{0.15}N_{0.99}$.

In order to verify the prediction that Mn doping at Zn site could induce the Γ^{5g} AFM ground state, the sample with refined compositions of $Mn_3Zn_{0.83}Mn_{0.15}N_{0.99}$ was synthesized and analyzed by NPD method. Figure 5(a) shows the NPD pattern of $Mn_3Zn_{0.83}Mn_{0.15}N_{0.99}$ at 10 K. The NPD pattern could be fitted well with a structural model of cubic symmetry and the Γ^{5g} AFM model, as shown in Figure 1(a). For Mn_3ZnN, it has been investigated previously, with a M_{PTE} magnetic ground state and a combination of Γ^{5g} and M_{PTE} AFM phases between 140 K and 177 K. Noticeably, our NPD study indicates that the ground state phase becomes Γ^{5g} symmetry in $Mn_3Zn_{0.83}Mn_{0.15}N_{0.99}$, suggesting that we could stabilize the Γ^{5g} AFM phase by Mn doping at Zn site. Moreover, the refined lattice constant a and AFM moment of Mn are 3.90274 Å and 2.60 μ_B/Mn, respectively, in $Mn_3Zn_{0.83}Mn_{0.15}N_{0.99}$, which are less than the values 3.912 Å and 2.61 μ_B/Mn in $Mn_3Zn_{0.99}N$.[27] This is in qualitative agreement with the calculated results that Mn doping could induce the decreasing of a and m_{Mn} in $Mn_3Zn_{0.875}Mn_{0.125}N$. On the other hand, the evolution of lattice constant and phase fractions with temperature is taken into consideration, as shown in Figure 5(b). Table S1 gives more details for the refined structural parameters of $Mn_3Zn_{0.83}Mn_{0.15}N_{0.99}$ compound at some representative temperature. For the phase fractions, the transition from Γ^{5g} AFM to PM is incomplete, and the Γ^{5g} phase fraction decreases gradually upon further heating and coexists with the PM phase between 130

and 140 K. Figure S3 provides supplementary details about the evolution of the NPD pattern with temperature. In addition, the MVE effect with magnetic transition from Γ^{5g} AFM (large volume) to PM (small volume) phases is observed as the previously calculated prediction. More importantly, the ZTE behavior is observed below 140 K within Γ^{5g} AFM phase, corresponding to the coefficient of linear thermal expansion α_l = 3.47×10^{-7} K^{-1}. This demonstrates that the ZTE behavior can be obtained by achieving the Γ^{5g} AFM phase in antiperovskite compounds.[26, 27]

Figure 5(c) gives the temperature dependence of the ordered magnetic moments (m_{Mn}) of Γ^{5g} AFM structure. The abrupt contraction in the volume is observed when m_{Mn} suddenly drops rapidly. This indicates a close correlation between the anomalous volume variation and the magnetic ordering, confirming the lattice is coupled to the Mn magnetic ordering.[26] Additionally, more details for the correlation between thermal expansion behaviors and intensities of the magnetic peak are shown in Figure S4 in the Supporting Information. In order to further investigate the spin-lattice coupling in the Γ^{5g} AFM phase, we assume that $\alpha_T(T) = \alpha_{PTE}(T)$ where $\alpha_T(T)$ and $\alpha_{PTE}(T)$ are defined as the coefficient of the usual thermal expansion contributed by the lattice vibration in the ZTE (blow 140 K) and PTE region (above 140 K), respectively. And the lattice constant $a_T(T)$ can be obtained from the fitting curve of PTE constants above 140 K using the cubic function (shown in the equation (1) of Supporting Information).[26, 27] Indicating $a(T)$ as the observed lattice constant, we take the difference $\Delta a_m(T) = a(T) - a_T(T)$ to isolate the effect of the NTE. As shown in the Figure 5(c), it can be seen that $\Delta a_m(T)$ of $Mn_3Zn_{0.83}Mn_{0.15}N_{0.99}$ at ZTE region decreases modestly with increasing temperature, but approximately at the same rate as the ordered moment decreasing. Therefore we define a ratio $r(T) = \Delta a_m(T)/m_{Mn}(T)$ as the extent of the NTE effect connected with the magnitude of the ordered moment $m_{Mn}(T)$. For $Mn_3Zn_{0.83}Mn_{0.15}N_{0.99}$, the ratio r(T), which is found to be a linear function with an extremely low coefficient value of -1.0822×10^{-5}, is approximately independent of T at the ZTE region. This reveals a strong spin-lattice coupling

phenomenon for Γ^{5g} AFM phase in $Mn_3Zn_{0.83}Mn_{0.15}N_{0.99}$, which has also been confirmed in Mn_3Zn_xN, $Mn_3Zn_{0.41}Ag_{0.41}N$ and $Mn_{3+x}Ni_{1-x}N$ antiperovskite compounds with Γ^{5g} AFM phase.[26, 27] This spin-lattice coupling could balance the contribution of the lattice vibration, and then produce ZTE behavior.

4. CONCLUSION

In summary, we have theoretically demonstrated that X doping at Zn site in $Mn_3Zn_{0.875}X_{0.125}N$ (X = Mn, Ge, and Sn) could stabilize the noncollinear Γ^{5g} AFM structure, and experimentally verify the prediction of Γ^{5g} AFM ground state (with Mn doping) that can be tunable to achieve ZTE behavior. Our calculated results with diverse EC functionals indicate that PW91 is the best one compared with others for the current study of Mn_3ZnN. Moreover, Γ^{5g} AFM ground state and NTE behavior that caused by MVE effect are confirmed in X (X = Ge, Sn, and Mn) doped $Mn_3Zn_{0.875}X_{0.125}N$. The reasons for collinear-noncollinear magnetic phase transition induced by doping are discussed based on local lattice distortion. In addition, from the NPD results of $Mn_3Zn_{0.83}Mn_{0.15}N_{0.99}$, the predicted Γ^{5g} AFM ground state and the ZTE caused by strong spin-lattice coupling are observed. The present study suggests that frustrated triangular magnetic systems with noncollinear Γ^{5g} AFM ground state are promising candidates for ZTE material with strong spin-lattice coupling in antiperovskite compounds.

■ ASSOCIATED CONTENT

Supporting Information

The total energies as a function of the lattice constant, some detailed analyses for the geometrical distortion, NPD patterns, cubic function of fitting curve, and refined structural parameters. The Supporting Information is available free of charge on the

ACS Publications website.

AUTHOR INFORMATION

Corresponding Authors

*E-mail: sunying@buaa.edu.cn.

*E-mail: congwang@buaa.edu.cn.

Notes

The authors declare no competing financial interest.

ACKNOWLEDGMENTS

This work is financially supported by the National Natural Science Foundation of China (NSFC) (Nos. 51172012 and 51472017), the Fundamental Research Funds for the Central Universities, and State Key Lab of Advanced Metals and Materials (2014-ZD03). The authors also acknowledge the support of Foundation of Beijing Municipal Science & Technology Commission (Z141109004414063).

REFERENCES

[1] Ye, F.; Fernandez-Baca, J. A.; Fishman, R. S.; Ren, Y.; Kang, H. J.; Qiu, Y.; Kimura, T. Magnetic Interactions in the Geometrically Frustrated Triangular Lattice Antiferromagnet $CuFeO_2$. *Phys. Rev. Lett.* **2007**, 99, 157201.

[2] Ramirez, A. P.; Hayashi, A.; Cava, R. J.; Siddharthan, R.; Shastry, B. S. Zero-Point Entropy in 'Spin Ice'. *Nature (London)* **1999**, 399, 333-335.

[3] Kimura, T.; Goto, T.; Shintani, H.; Ishizaka, K.; Arima, T.; Tokura, Y. Magnetic Control of Ferroelectric Polarization. *Nature (London)* **2003**, 426, 55-58.

[4] Hur, N.; Park, S.; Sharma, P. A.; Ahn, J. S.; Guha, S.; Cheong, S-W. Electric

Polarization Reversal and Memory in a Multiferroic Material Induced by Magnetic Fields. *Nature (London)* **2004**, 429, 392-395.

[5] Lottermoser, T.; Lonkai, T.; Amann, U.; Hohlwein, D.; Ihringer, J.; Fiebig, M. Magnetic Phase Control by an Electric Field. *Nature (London)* **2004**, 430, 541-544.

[6] Diep, H. T. *Frustrated Spin Systems*. World Scientific: Singapore, 2005.

[7] Melchy, P. -É.; Zhitomirsky, M. E. Interplay of Anisotropy and Frustration: Triple Transitions in a Triangular-Lattice Antiferromagnet. *Phys. Rev. B* **2009**, 80, 064411.

[8] Landsgesell, S.; Prokeš, K.; Ouladdiaf, B.; Klemke, B.; Prokhnenko, O.; Hepp, B.; Kiefer, K.; Argyriou, D. N. Magnetoelectric Properties in Orthorhombic $Nd_{1-x}Y_xMnO_3$: Neutron Diffraction Experiments. *Phys. Rev. B* **2012**, 86, 054429.

[9] Cheong, S.-W.; Mostovoy, M. Multiferroics: a Magnetic Twist for Ferroelectricity. *Nat. Mater.* **2007**, 6, 13-20.

[10] Reja, S.; Ray, R.; Brink, J.; Kumar, S. Coupled Spin-Charge Order in Frustrated Itinerant Triangular Magnets. *Phys. Rev. B* **2015**, 91, 140403(R).

[11] Salamon, M.; Jaime, M. The Physics of Manganites: Structure and Transport. *Rev. Mod. Phys.* **2001**, 73, 583-628.

[12] Nagaosa, N.; Sinova, J.; Onoda, S.; MacDonald, A. H.; Ong, N. P. Anomalous Hall Effect. *Rev. Mod. Phys.* **2010**, 82, 1539-1592.

[13] Wang, R. F.; Nisoli, C.; Freitas, R. S.; Li, J.; McConville, W.; Cooley, B. J.; Lund, M. S.; Samarth, N.; Leighton, C.; Crespi, V. H.; Schiffer, P. Artificial 'Spin Ice' in a Geometrically Frustrated Lattice of Nanoscale Ferromagnetic Islands. *Nature (London)* **2006**, 439, 303-306.

[14] Nisoli, C.; Moessner, R.; Schiffer, P. Colloquium: Artificial Spin Ice: Designing and Imaging Magnetic Frustration. *Rev. Mod. Phys.* **2013**, 85, 1473-1490.

[15] Hayami, S.; Motome, Y. Multiple-Q Instability by (d-2)-Dimensional Connections of Fermi Surfaces. *Phys. Rev. B* **2014**, 90, 060402.

[16] Kimura, T.; Lashley, J. C.; Ramirez, A. P. Inversion-Symmetry Breaking in the Noncollinear Magnetic Phase of the Triangular-Lattice Antiferromagnet $CuFeO_2$. *Phys. Rev. B* **2006**, 73, 220401(R).

[17] Yu, M. H.; Lewis, L. H.; Moodenbaugh, A. R. Large Magnetic Entropy Change in

the Metallic Antiperovskite Mn_3GaC. *J Appl. Phys.* **2003**, 93, 10128-10130.

[18] Yan, J.; Sun, Y.; Wu, H.; Huang, Q. Z.; Wang, C.; Shi, Z. X.; Deng, S. H.; Shi, K. W.; Lu, H. Q.; Chu, L. H. Phase Transitions and Magnetocaloric Effect in $Mn_3Cu_{0.89}N_{0.96}$. *Acta Mater.* **2014**, 74, 58-65.

[19] Fruchart, D.; Bertaut, E. F. Magnetic Studies of the Metallic Perovskite-Type Compounds of Manganese. *J. Phys. Soc. Jpn.* **1978**, 44, 781-791.

[20] Shimizu, T.; Shibayama, T.; Asano, K.; Takenaka, K. Giant Magnetostriction in Tetragonally Distorted Antiperovskite Manganese Nitrides. *J. Appl. Phys.* **2012**, 111, 07A903.

[21] Shibayama, T.; Takenaka, K. Giant Magnetostriction in Antiperovskite Mn_3CuN. *J. Appl. Phys.* **2011**, 109, 07A928.

[22] Sun, Y.; Guo, Y. F.; Tsujimoto, Y.; Wang, C.; Li, J.; Wang, X.; Feng, H. L.; Sathish, C. I.; Matsushita, Y.; Yamaura, K. Unusual Magnetic Hysteresis and the Weakened Transition Behavior Induced by Sn Substitution in Mn_3SbN. *J. Appl. Lett.* **2014**, 115, 043509.

[23] Kamishima, K.; Goto, T.; Nakagawa, H.; Miura, N.; Ohashi, M.; Mori, N. Giant Magnetoresistance in the Intermetallic Compound Mn_3GaC. *Phys. Rev. B* **2000**, 63, 024426.

[24] Matsunami, D.; Fujita, A.; Takenaka, K.; Kano, M. Giant Barocaloric Effect Enhanced by the Frustration of the Antiferromagnetic Phase in Mn_3GaN. *Nat. Mater.* **2015**, 14, 73-78.

[25] Lukashev, P.; Sabirianov, R. F.; Belashchenko, K. Theory of the Piezomagnetic Effect in Mn-based Antiperovskites. *Phys. Rev. B* **2008**, 78, 184414.

[26] Deng, S. H.; Sun, Y.; Wu, H.; Huang, Q. Z.; Yan, J.; Shi, K. W.; Malik, M. I.; Lu, H. Q.; Wang, L.; Huang, R. J.; Li, L. F.; Wang, C. Invar-like Behavior of Antiperovskite $Mn_{3+x}Ni_{1-x}N$ Compounds. *Chem. Mater.* **2015**, 27, 2495-2501.

[27] Wang, C.; Chu, L. H.; Yao, Q. R.; Sun, Y.; Wu, M. M.; Ding, L.; Yan, J.; Na, Y. Y.; Tang, W. H.; Li, G. N.; Huang, Q. Z.; Lynn, J. W. Tuning the Range, Magnitude, and Sign of the Thermal Expansion in Intermetallic $Mn_3(Zn, M)_xN$ (M = Ag, Ge). *Phys. Rev. B* **2012**, 85, 220103(R).

[28] Iikubo, S.; Kodama, K.; Takenaka, K.; Takagi, H.; Takigawa, M.; Shamoto, S. Local Lattice Distortion in the Giant Negative Thermal Expansion Material

$Mn_3Cu_{1-x}Ge_xN$. *Phys. Rev. Lett* **2008**, 101, 205901.

[29] Song, X. Y.; Sun, Z. H.; Huang, Q. Z.; Rettenmayr, M.; Liu, X. M.; Seyring, M.; Li, G. N.; Rao, G. H.; Yin, F. X. Adjustable Zero Thermal Expansion in Antiperovskite Manganese Nitride. *Adv. Mater.* **2011**, 23, 4690-4694.

[30] Hamada, T.; Takenaka, K. Phase Instability of Magnetic Ground State in Antiperovskite Mn_3ZnN: Giant Magnetovolume Effects Related to Magnetic Structure. *J. Appl. Phys.* **2012**, 111, 07A904.

[31] Fruchart, R.; Madar, R.; Barberon, M.; Fruchart, E.; Lorthioir, M. G. Transitions Magnétiques et Déformations Cristallographiques Associées Dans les Nitrures du Type Perowskite $ZnMn_3N$ et $SnMn_3N$. *J. Phys. (Paris)* **1971**, 32, 982-984.

[32] Sun, Y.; Wang, C.; Wen, Y. C.; Zhu, K. G.; Zhao J. T. Lattice Contraction and Magnetic and Electronic Transport Properties of $Mn_3Zn_{1-x}Ge_xN$. *Appl. Phys. Lett.* **2007**, 91, 231913.

[33] Sun, Y.; Wang, C.; Wen, Y. C.; Chu, L. H.; Pan, H.; Nie, M. Negative Thermal Expansion and Magnetic Transition in Anti-Perovskite Structured $Mn_3Zn_{1-x}Sn_xN$ Compounds. *J. Am. Ceram. Soc.* **2010**, 93, 2178-2181.

[34] Ma, P. W.; Dudarev, S. L. Constrained Density Functional for Noncollinear Magnetism. *Phys. Rev. B* **2015**, 91, 054420.

[35] Mryasov, O. N.; Gubanov, V. A.; Liechtenstein, A. I. Spiral-Spin-Density-Wave States in Fcc Iron: Linear-Muffin-Tin-Orbitals Band-Structure Approach. *Phys. Rev. B* **1992**, 45, 12330.

[36] Mryasov, O. N.; Lichtenstein, A. I.; Sandratskii, L. M.; Gubanov, V. A. Magnetic Structure of FCC Iron. *J. Phys. Condens. Matter* **1991**, 3, 7683-7690.

[37] Lukashev, P.; Belashchenko, K. D.; Sabirianov, R. F. Large Magnetoelectric Effect in Ferroelectric/Piezomagnetic Heterostructures. *Phys. Rev. B* **2011**, 84, 134420.

[38] Blöchl, P. Projector Augmented-Wave Method. *Phys. Rev. B*, **1994**, 50, 17953-17979.

[39] Kresse, G.; Joubert, D. From Ultrasoft Pseudopotentials to the Projector Augmented-Wave Method. *Phys. Rev. B* **1999**, 59, 1758-1775.

[40] Perdew, J. P.; Wang, Y. Accurate and Simple Analytic Representation of the Electron-Gas Correlation Energy. *Phys. Rev. B* **1992**, 45, 13244-13249.

[41] Perdew, J. P.; Burke, K.; Ernzerhof, M. Generalized Gradient Approximation Made Simple. *Phys. Rev. Lett.* **1996**, 77, 3865-3868.

[42] Mattsson, A. E.; Armiento, R.; Paier, J.; Kresse, G.; Wills, J. M.; Mattsson, T. R. The AM05 Density Functional Applied to Solids. *J. Chem. Phys.* **2008**, 128, 084714.

[43] Ropo, M.; Kokko, K.; Vitos, L. Assessing the Perdew-Burke-Ernzerhof Exchange-Correlation Density Functional Revised for Metallic Bulk and Surface Systems. *Phys. Rev. B* **2008**, 77, 195445.

[44] Liu, C. M.; Chen, X. R.; Xu, C.; Cai, L. C.; Jing, F. Q. Melting Curves and Entropy of Fusion of Body-Centered Cubic Tungsten Under Pressure. *J. Appl. Phys.* **2012**, 112, 013518.

[45] Humphrey, W.; Dalke, A.; Schulten, K. VMD - Visual Molecular Dynamics, *J. Molec. Graphics* **1996**, 14, 33-38.

[46] Larson, A. C.; Von Dreele, R. B. *General Structure Analysis System (GSAS)*, Technical Report LAUR 86-748 for Los Alamos National Laboratory: Los Alamos, NM, 2004.

[47] Qu, B. Y.; Pan, B. C. Nature of the Negative Thermal Expansion in Antiperovskite Compound Mn_3ZnN. *J. Appl. Phys.* **2010**, 108, 113920.

[48] Sun, Y.; Wang, C.; Huang, Q. Z.; Guo, Y. F.; Chu, L. H.; Arai, M. S.; Yamaura, K. Neutron Diffraction Study of Unusual Phase Separation in the Antiperovskite Nitride Mn_3ZnN. *Inorg. Chem.* **2012**, 51, 7232-7236.

[49] Granado, E.; Huang, Q.; Lynn, J. W.; Gopalakrishnan, J.; Greene, R. L.; Ramesha, K. Spin-Orbital Ordering and Mesoscopic Phase Separation in the Double Perovskite Ca_2FeReO_6. *Phys. Rev. B* **2002**, 66, 064409.

[50] Terada, N.; Nakajima, T.; Mitsuda, S.; Kitazawa, H.; Kaneko, K.; Metoki, N. Ga-Substitution-Induced Single Ferroelectric Phase in Multiferroic $CuFeO_2$. *Phys. Rev. B* **2008**, 78, 014101.

[51] Hua, L.; Wang, L.; Chen, L. F. First-Principles Investigation of Ge Doping Effects on the Structural, Electronic and Magnetic Properties in Antiperovskite Mn_3CuN. *J. Phys.: Condens. Matter* **2010**, 22, 206003.

[52] Fishman, R. S.; Okamoto, S. Noncollinear Magnetic Phases of a Triangular-Lattice Antiferromagnet and of Doped $CuFeO_2$. *Phys. Rev. B* **2010**, 81, 020402(R).

[53] Wang, F.; Vishwanath, A. Spin Phonon Induced Collinear Order and Magnetization Plateaus in Triangular and Kagome Antiferromagnets: Applications to $CuFeO_2$. *Phys. Rev. Lett.* **2008**, 100, 077201.

[54] Kawamura, H. Universality of Phase Transitions of Frustrated Antiferromagnets. *J. Phys. Condens. Matter* **1998**, 10, 4707-4754.

[55] Fishman, R. S. Spin Waves in $CuFeO_2$. *J. Appl. Phys.* **2008**, 103, 07B109.

[56] Seki, S.; Yamasaki, Y.; Shiomi, Y.; Iguchi, S.; Onose, Y.; Tokura, Y. Intrinsic Damping of Spin Waves by Spin Current in Conducting Two-Dimensional Systems. *Phys. Rev. B* **2007**, 75, 100403(R).

Table of Contents

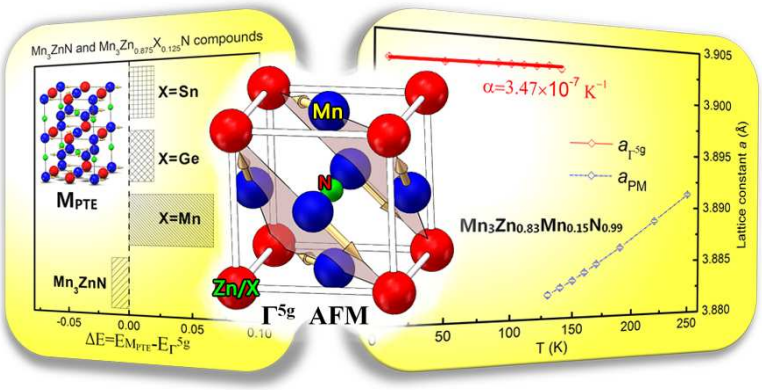

	LDA	AM05	PBEsol	PBE	PW91	Experiment
a_0 (Å)	3.702	3.781	3.790	3.871, 3.870[44]	3.860	3.912[27]
m (μ_B)	2.21	2.10	2.16	2.60, 2.63[44]	2.51	2.61[27]

Table 1 for manuscript
108x35mm (300 x 300 DPI)

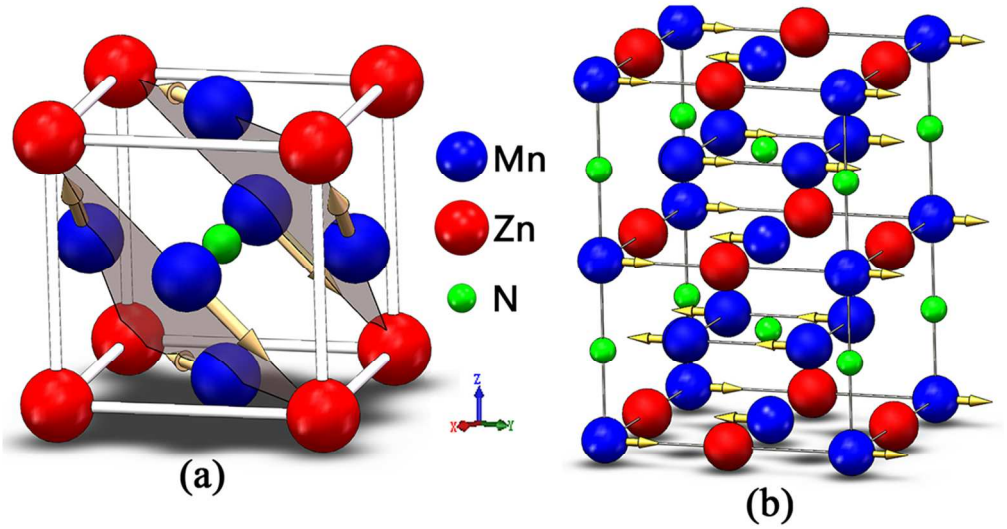

Figure 1 for manuscript
102x56mm (300 x 300 DPI)

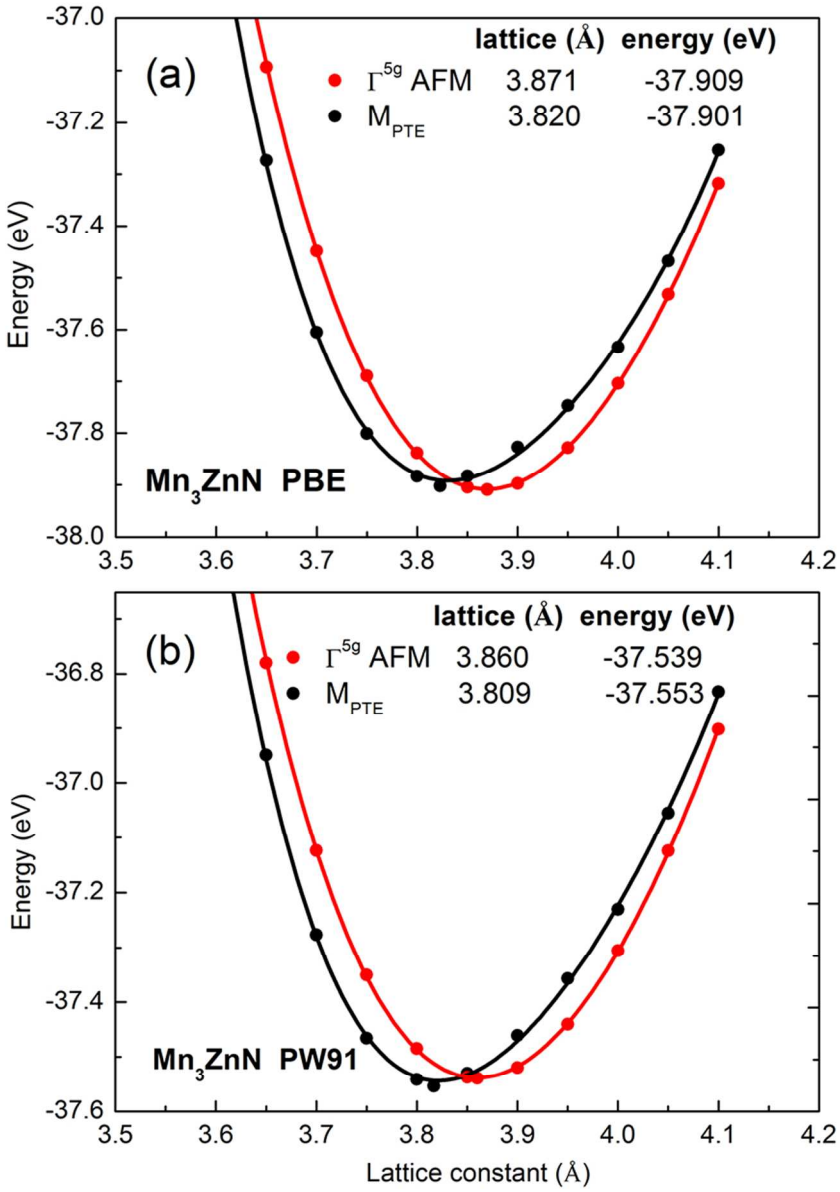

Figure 2 for manuscript
75x105mm (300 x 300 DPI)

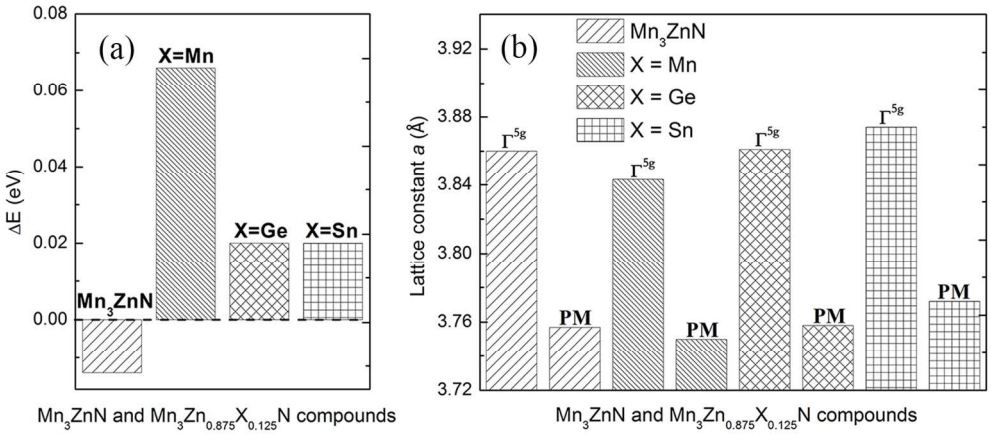

Figure 3 for manuscript
150x66mm (300 x 300 DPI)

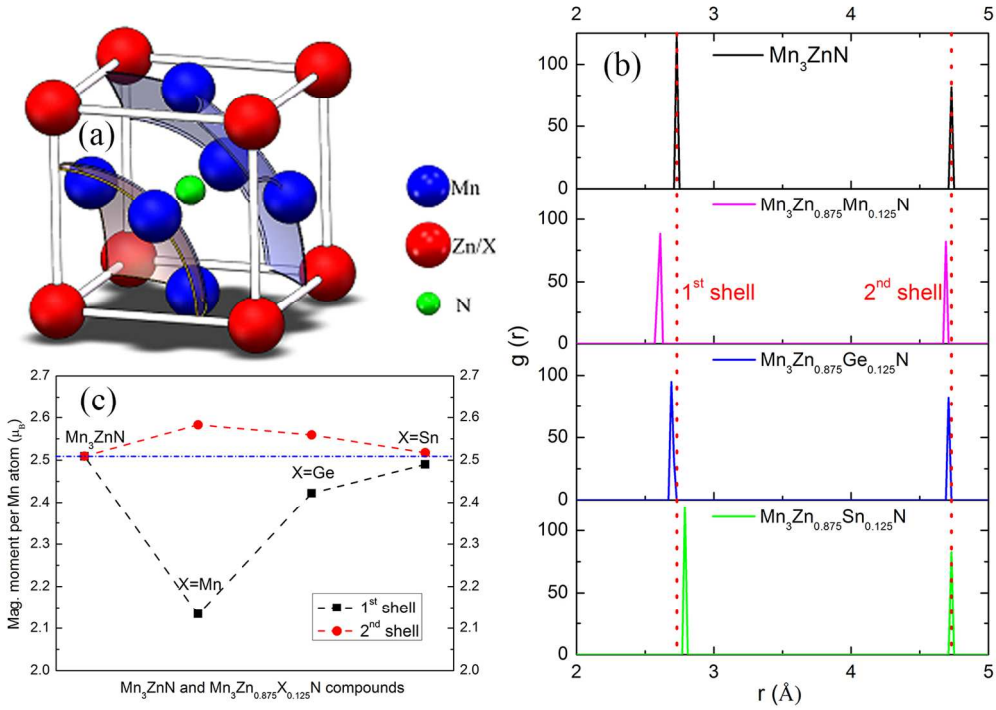

Figure 4 for manuscript
146x104mm (300 x 300 DPI)

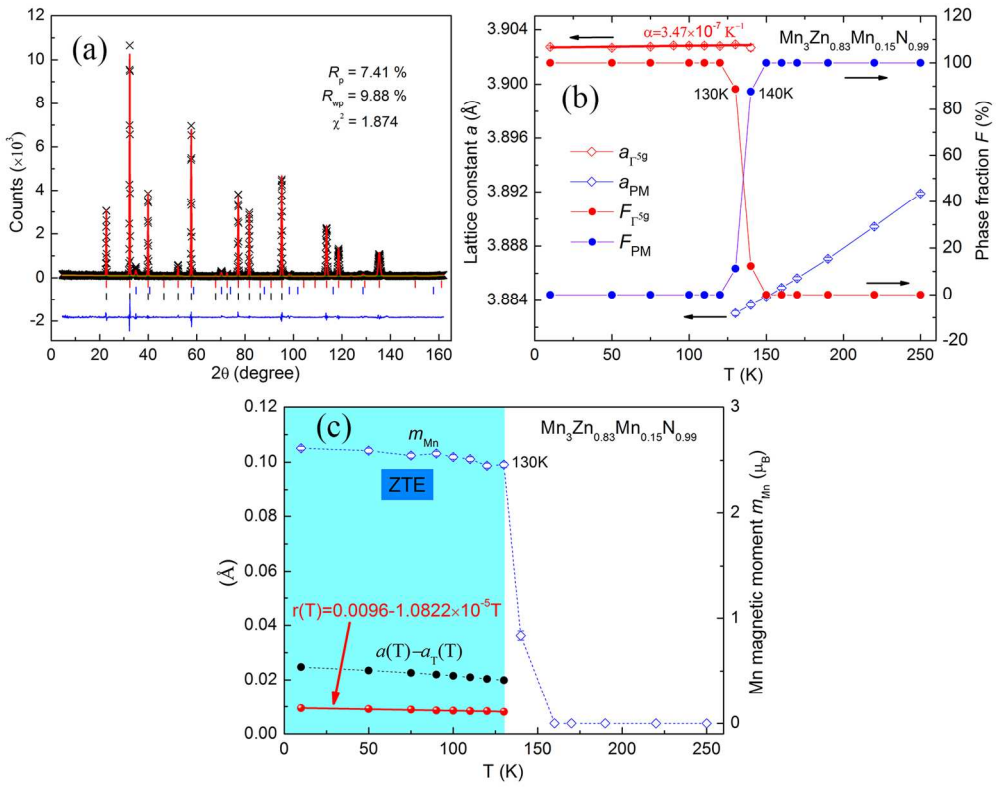

Figure 5 for manuscript
150x117mm (300 x 300 DPI)

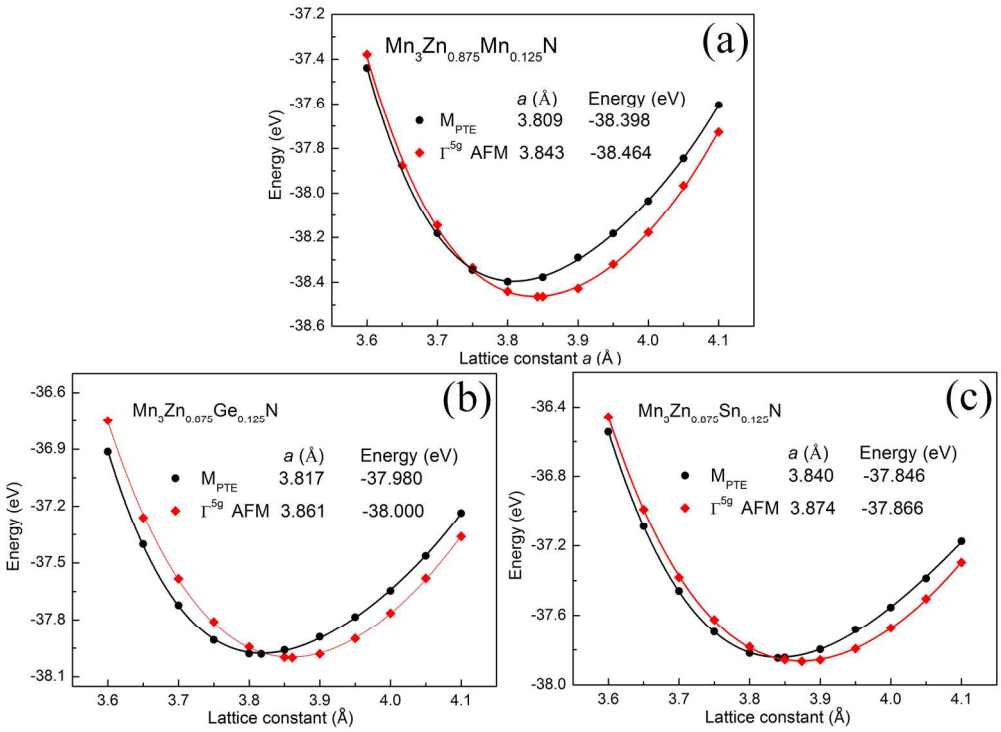

Figure S1 for Supporting information
172x125mm (300 x 300 DPI)

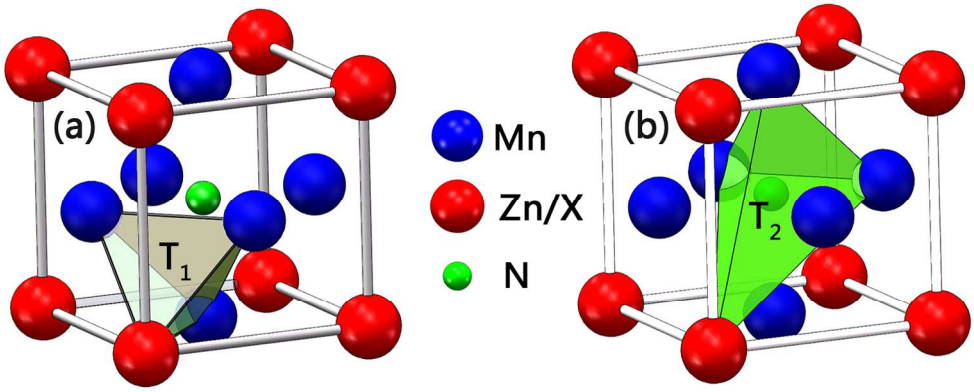

Figure S2 for Supporting information
141x57mm (300 x 300 DPI)

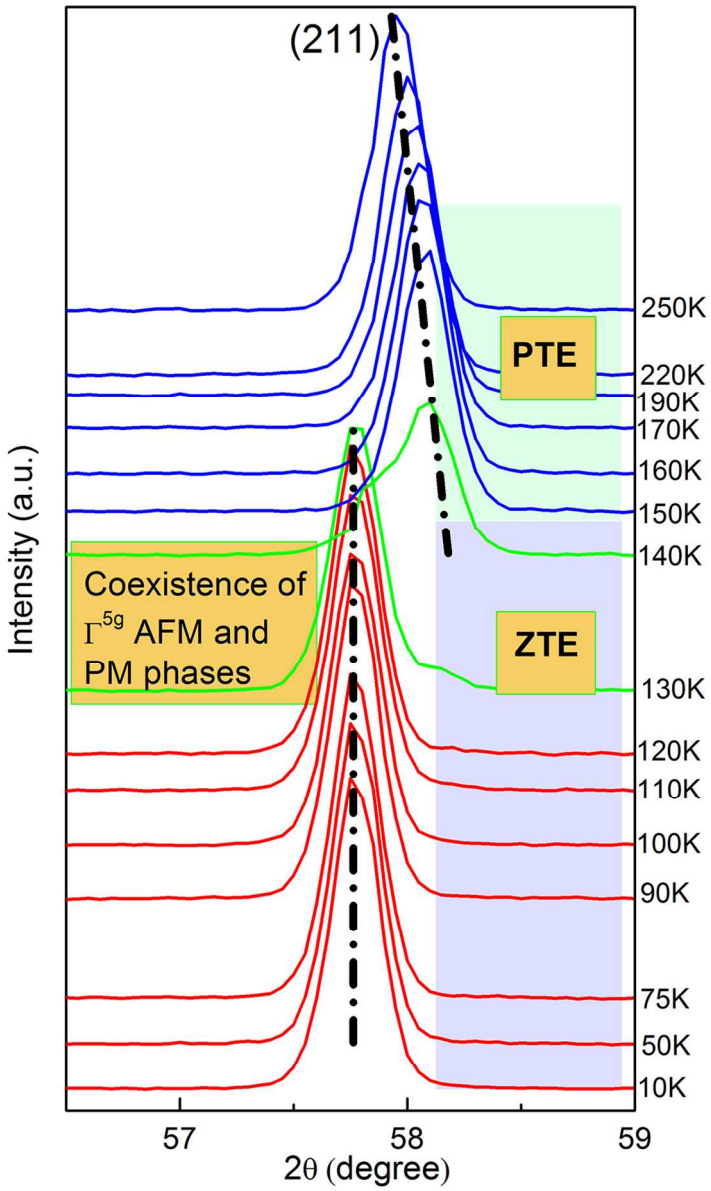

Figure S3 for Supporting information
96x147mm (300 x 300 DPI)

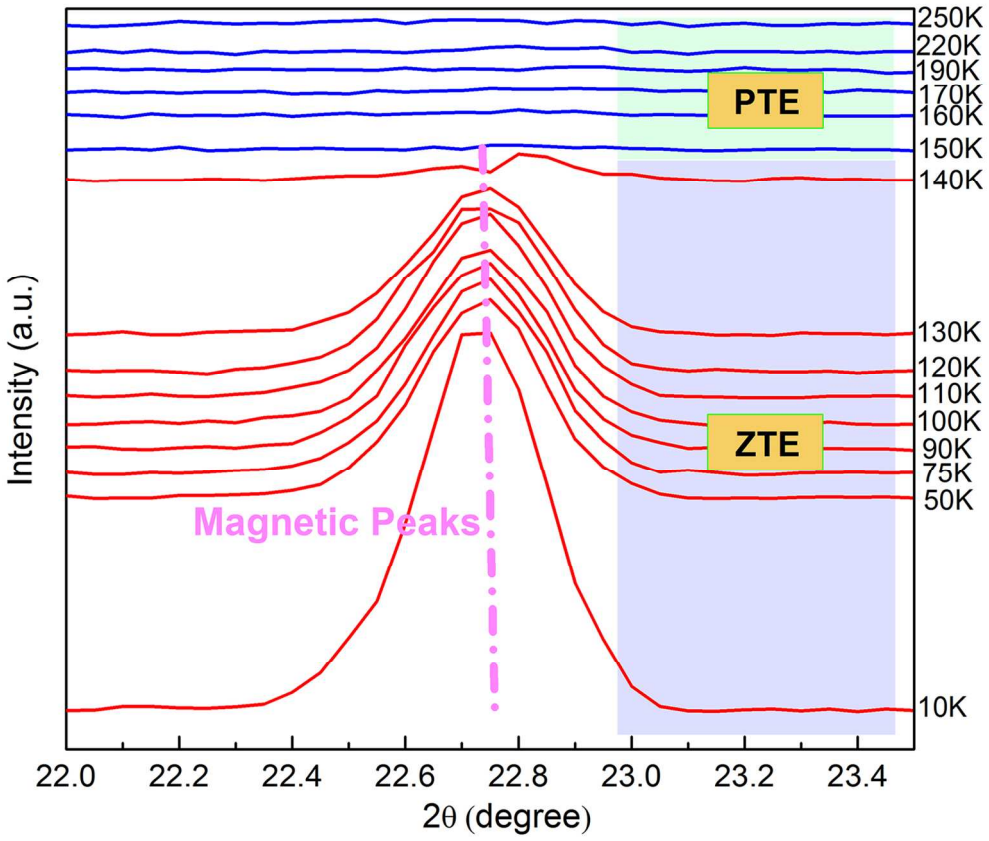

Figure S4 for Supporting information
134x117mm (300 x 300 DPI)

T (K)	a	Err a	m_{Mn}	Err m_{Mn}	R (%)	R_{wp} (%)	χ^2 (%)	U_{iso} (Mn)	U_{iso} (Zn)	U_{iso} (N)
10	3.90274	8×10^{-5}	2.60	0.02	7.41	9.88	1.874	3.01×10^{-3}	3.50×10^{-3}	1.40×10^{-3}
110	3.90284	9×10^{-5}	2.51	0.02	6.78	8.76	1.265	3.60×10^{-3}	3.79×10^{-3}	2.30×10^{-3}
170	3.8856	1×10^{-4}	0	-	7.86	8.81	1.543	5.16×10^{-3}	5.21×10^{-3}	2.84×10^{-3}
250	3.8919	1×10^{-4}	0	-	6.26	7.31	1.342	5.25×10^{-3}	6.54×10^{-3}	3.94×10^{-3}

Table S1 for Supporting information
109x38mm (300 x 300 DPI)

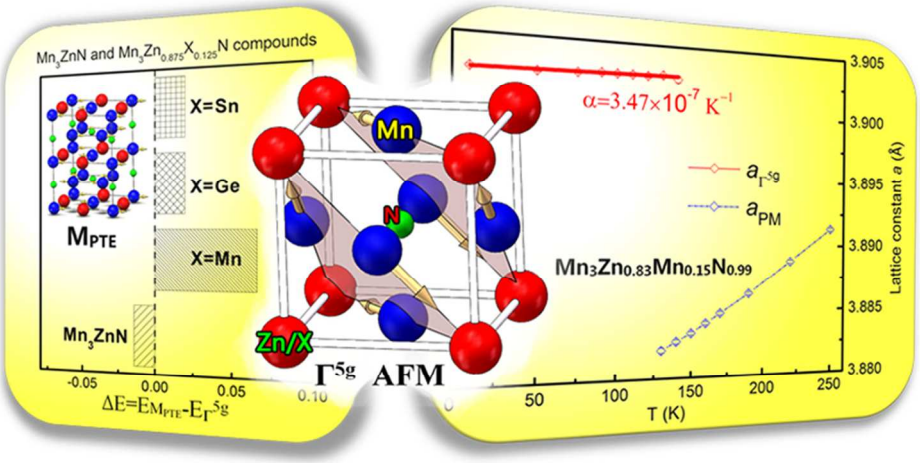

Table of Contents for manuscript
74x35mm (300 x 300 DPI)